

# Faradaically selective membrane for liquid metal displacement batteries

Huayi Yin<sup>1,2</sup>, Brice Chung<sup>1</sup>, Fei Chen<sup>1,3</sup>, Takinari Ouchi<sup>1</sup>, Ji Zhao<sup>1</sup>, Nobuyuki Tanaka<sup>1,4</sup> and Donald R. Sadoway<sup>1\*</sup>

**In the realm of stationary energy storage, a plurality of candidate chemistries continues to vie for acceptance, among them the Na–NiCl<sub>2</sub> displacement battery, which has eluded widespread adoption owing to the fragility of the β''-Al<sub>2</sub>O<sub>3</sub> membrane. Here we report a porous electronically conductive membrane, which achieves chemical selectivity by preferred faradaic reaction instead of by regulated ionic conduction. Fitted with a porous membrane of TiN, a displacement cell comprising a liquid Pb positive electrode, a liquid Li–Pb negative electrode and a molten-salt electrolyte of PbCl<sub>2</sub> dissolved in LiCl–KCl eutectic was cycled at a current density of 150 mA cm<sup>-2</sup> at a temperature of 410 °C and exhibited a coulombic efficiency of 92% and a round-trip energy efficiency of 71%. As an indication of industrial scalability, we show comparable performance in a cell fitted with a faradaic membrane fashioned out of porous metal.**

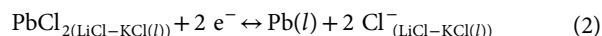
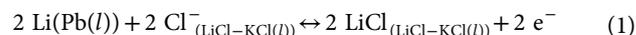
Stationary storage is a technology that mitigates the intermittency of renewable sources of energy such as wind and photovoltaic solar. Furthermore, the existing grid would benefit from stationary storage in terms of greater resiliency and lower emissions as well as better utilization of assets (generation, transmission and distribution)<sup>1–4</sup>. An attractive candidate in this regard is the Na–NiCl<sub>2</sub> chemistry whose origins can be traced back to the discovery by Kummer and Weber that β''-Al<sub>2</sub>O<sub>3</sub> is a Na-ion conductor, which meant that liquid sodium could function as a negative electrode in a battery, the first being sodium–sulfur<sup>5</sup>. Subsequently, Coetzer paired liquid sodium with an electrode of NiCl<sub>2</sub> supported by Ni metal and flooded the space between it and the β''-Al<sub>2</sub>O<sub>3</sub> membrane with molten NaAlCl<sub>4</sub> (ref. 6). In spite of its fine attributes, this battery has not achieved widespread market penetration<sup>7–10</sup>. The fragility and brittleness of the β''-Al<sub>2</sub>O<sub>3</sub> combined with its vulnerability to attack by transition-metal ions in a chloroaluminate melt put severe constraints on cell design, which, in turn, limit performance<sup>11</sup>. This seems to be the case for U-shaped tube configurations of β''-Al<sub>2</sub>O<sub>3</sub> as well as for large-area planar configurations of this material<sup>12–14</sup>.

In a departure from the classical ceramic single-ion conductor, here we report the use of a porous electronically conductive membrane (Fig. 1), which achieves chemical selectivity by preferred faradaic reduction of vulnerable transition-metal ions (here Pb<sup>2+</sup> is reduced to liquid metal to prevent Pb from entering the negative electrode) while at the same time the pores of the membrane allow for transport of cations of the active metal of the negative electrode (Li<sup>+</sup> here) as well as anions of the molten-salt electrolyte (Cl<sup>-</sup> here). The electrons that reduce the Pb<sup>2+</sup> are produced by the oxidation of Li (labelled anode reaction). As needed, a fraction of such electrons traverse the electronically conductive membrane in order to drive the faradaic protection reaction on its lower surface. With this faradaically active membrane, we have unlocked both the choice of the negative electrode (not bound to liquid Na) and the choice of the positive electrode (not restricted to solid metals that form solid halides). The

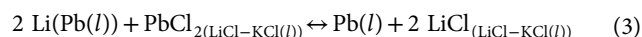
result is an operative all-liquid (metals and salts) displacement chemistry that we name the liquid displacement battery (LDB).

## The thermodynamics of the liquid displacement battery

The example of a Li–Pb||PbCl<sub>2</sub> cell (Fig. 1), comprising a liquid Li–Pb negative electrode where Li is the active metal and Pb is a host metal, a molten-salt electrolyte of LiCl–KCl eutectic with dissolved PbCl<sub>2</sub> and a liquid Pb positive electrode, was chosen based on the thermodynamics of the binary liquid Li–Pb system<sup>15</sup> and on our own measurements of the electrochemistry of Pb/Pb<sup>2+</sup> displacement reactions in molten LiCl–KCl. The half-cell reactions are:



The overall cell displacement reaction is:



On charging, Pb in the positive electrode oxidizes to Pb<sup>2+</sup> ion, which dissolves in the LiCl–KCl electrolyte. In parallel, on the negative electrode, Li<sup>+</sup> ions in the electrolyte are reduced to Li metal, which alloys with the Pb host. The problem is that direct contact between the dissolved Pb<sup>2+</sup> and the Li–Pb negative electrode would result in a spontaneous reaction ( $2 \text{Li}_{\text{in Pb}} + \text{Pb}^{2+} \rightarrow \text{Li–Pb} + 2 \text{Li}^+$ ) and permanent transfer of Pb into the negative electrode with attendant loss of energy storage capacity. It is for this reason that ZEBRA resorts to the choice of Ni for the positive electrode, as NiCl<sub>2</sub> is insoluble in NaAlCl<sub>4</sub>. Coetzer himself wrote ‘A crucial feature of the positive electrode reaction is that it requires the electrochemically active species to be effectively insoluble in the molten salt electrolyte. The electrochemically active material must always remain “pinned” to the electronically conductive backbone matrix,

<sup>1</sup>Department of Materials Science and Engineering, Massachusetts Institute of Technology, Cambridge, MA, USA. <sup>2</sup>School of Metallurgy, Northeastern University, Shenyang, China. <sup>3</sup>State Key Lab of Advanced Technology for Materials Synthesis and Processing, Wuhan University of Technology, Wuhan, China. <sup>4</sup>Nuclear Hydrogen & Heat Application Research Center, Japan Atomic Energy Agency, Ibaraki, Japan. Huayi Yin, Brice Chung, Fei Chen and Takinari Ouchi contributed equally to this work. \*e-mail: [dsadoway@mit.edu](mailto:dsadoway@mit.edu)

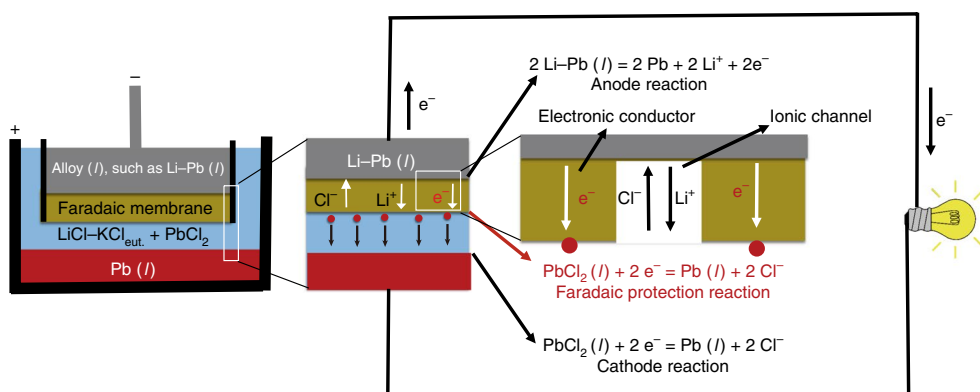


**Fig. 1 | Schematic of displacement cell discharging.** A Li-Pb||PbCl<sub>2</sub> cell fitted with a porous faradaically selective membrane. Depicted are the anode reaction at the interface between the liquid Li-Pb and the top surface of the membrane, the cathode reaction at the interface between the liquid Pb and the electrolyte, and the faradaic protection reaction at the membrane/electrolyte interface.

which can be unreacted metal itself<sup>6</sup>. The consequence of the latter is that, on charging, the positive electrode becomes coated with an ever-thickening solid layer of insulating metal halide, which ultimately halts current flow and prevents full utilization of the positive electrode. On discharge, when the cell is near a full state of charge, this same solid insulating halide layer constrains power delivery. To permit the use of a liquid metal positive electrode that converts to a metal halide that is soluble in the molten-salt electrolyte, we fit the cell not with an ion-selective ceramic membrane but rather with a porous electronically conductive membrane, so that the arrival of Pb<sup>2+</sup> at the lower surface of the membrane is accompanied by

faradaic reduction to Pb metal before it can alloy with the negative electrode. On discharge, electron transfer to Pb<sup>2+</sup> is supported by the oxidation of Li from the Li-Pb negative electrode. Li<sup>+</sup> ions enter the electrolyte in the pores of the membrane (serving as ionic channels), while the electrons have two pathways. The dominant pathway is the external circuit taking more than 90% of the total current, which, in turn, is reflected in the measured value of coulombic efficiency. The second pathway is through the electronically conductive membrane, which facilitates faradaic reduction of Pb<sup>2+</sup> at the interface of the electrolyte/membrane, blocking the transport of Pb<sup>2+</sup> to the Li-Pb pool above, and confining the liquid Pb to the positive electrode chamber. The newly reduced Pb coalesces into droplets that fall to the Pb pool at the bottom of the cell. It is this faradaic reaction that blocks permeation of Pb<sup>2+</sup> through the membrane, thereby vitiating metallothermic reduction and consequent irreversible loss of cell capacity. The difference in concentration of Pb<sup>2+</sup> at opposite levels of the electrolyte (that is, highest adjacent to the positive electrode and zero at the lower surface of the faradaic membrane) ensures that the magnitude of this blocking current remains acceptably small so as not to render cell operation impractical. The use of Pb host metal in the negative electrode serves to limit the concentration of Li so as to avert on the lower surface of the membrane the generation of pure Li metal and the formation of solid intermetallic compounds of Li-Pb. Admittedly, such use of a host metal in the anode reduces the cell voltage. The open-circuit voltage for equation (3) is the difference between the potentials of Li-Pb and Pb/PbCl<sub>2</sub>. The potential on the negative electrode spans the range from 0 to 0.8 V versus pure Li, varying with the concentration of Li in Pb (ref. <sup>15</sup>). The standard potential on the positive electrode, Pb/PbCl<sub>2</sub> versus Li, is 2.31 V at 410 °C (HSC Chemistry 6.0). Depending on the concentration of Pb<sup>2+</sup> in the electrolyte, the positive electrode potential varies from 0.8 to 2.31 V. Under the operating conditions in this work, the nominal open-circuit voltage of the cell was around 1.5 V, as indicated in Supplementary Fig. 1. There is room for optimization of cell voltage by regulating the concentration of Pb in the negative electrode and the concentration of Pb<sup>2+</sup> in the electrolyte.

This shift in selectivity from ionic mobility to faradaic reaction unfetters the chemistry of the displacement battery in two significant ways. First, such a displacement cell can operate with a liquid metal positive electrode that converts to a halide that is itself soluble in the molten-salt electrolyte. This means that the interface between the positive electrode and the molten-salt electrolyte remains unobstructed at all times. Accordingly, the mass transport kinetics at such a liquid/liquid interface are dramatically faster than those at a three-phase liquid/solid/solid interface, resulting in much higher current rates throughout the cycle on both charge and discharge<sup>16</sup>.

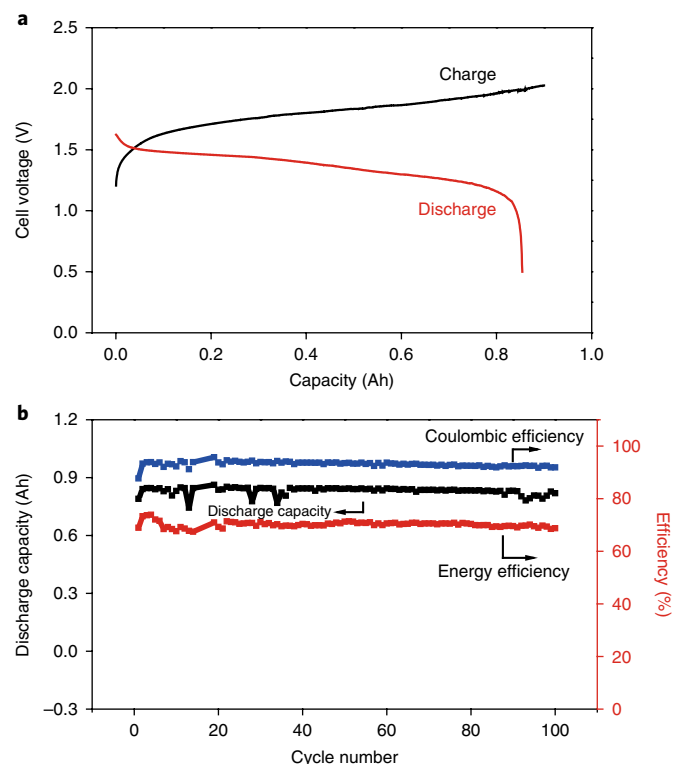


**Fig. 2 | Performance of a Li-Pb||PbCl<sub>2</sub> cell.** **a**, Voltage-time traces, charge and discharge. **b**, Discharge capacity, energy efficiency and coulombic efficiency as a function of cycle number. Operating temperature, 410 °C. Current density, 150 mA cm<sup>-2</sup>.

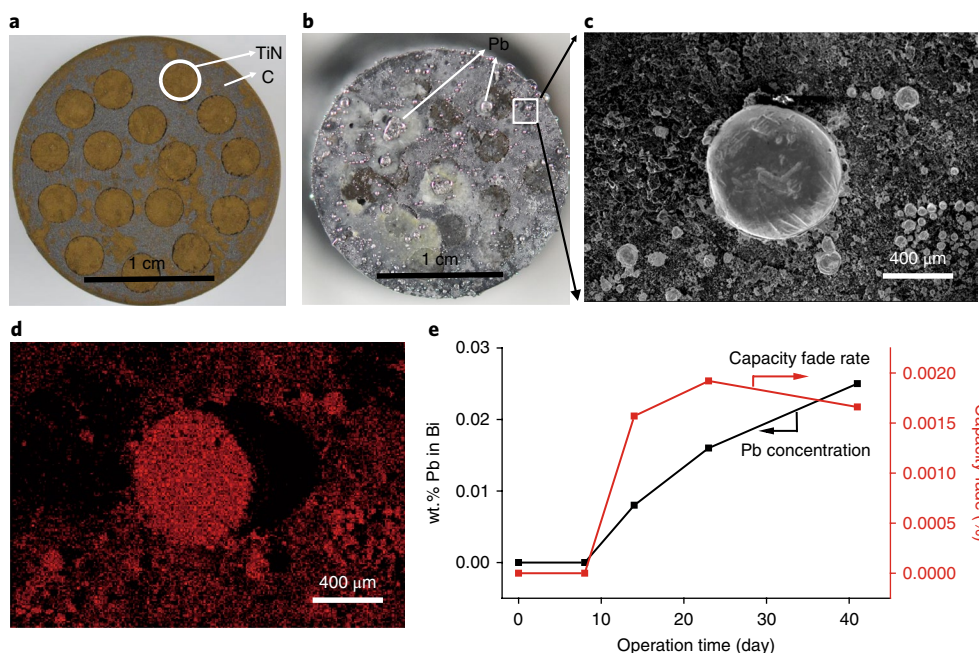
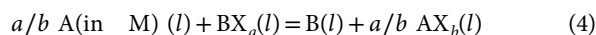


**Fig. 3 | Chemical analysis of a Pb droplet on the lower surface of the membrane and of the Pb permeation rate through the membrane.** **a, b**, Images of the bottom view of a porous TiN membrane before **(a)** and after **(b)** 100 cycles. **c**, SEM image of the area indicated in **b**. **d**, EDS mapping of **c**, showing the presence of Pb (in red). **e**, Pb concentration and the calculated capacity fade rate as a function of service lifetime.

Secondly, the negative electrode need not be liquid Na. This gives access to a large array of choices without relying on the discovery of concomitant ion-selective ceramic membranes. The overall reaction of the A–M||BX displacement cell can be written as follows:



where A is a low-melting, strongly electropositive metal or alloy of the same (for example, Li, Na, Mg, Al), M and B are low-melting, strongly electronegative metals or alloys of the same (for example, Sn, Sb, Pb, Bi, Zn), X is a strongly electronegative non-metal or solution of the same (for example, F, Cl, Br, I),  $a$  is the valence of the electronegative metal ion and  $b$  is the valence of the electropositive metal ion. The porous membrane is electronically conductive and resistant to chemical attack by the molten salt containing ions of the electronegative metal (positive electrode). Furthermore, we show that the faradaic membrane can be fashioned out of metal so as to be mechanically durable, which suggests that it may be easily mass-produced at large scale with a thin cross-section for minimal ohmic drop in cell voltage.

### Charge–discharge cycle testing of LDB chemistries

Figure 2 shows the performance of an LDB cell comprising a Pb positive electrode, a Li–Pb negative electrode and a molten-salt electrolyte of  $\text{PbCl}_2$  dissolved in LiCl–KCl eutectic. The negative electrode is contained in a closed-one-end graphite tube, the bottom of which has 16 3-mm holes that contain sintered TiN powder (Fig. 3a), a material selected for its known resistance to chemical attack by Li but an unlikely choice owing to the fact that TiN is an electronic conductor. Figure 2a shows the voltage–time traces on charging and discharging at a current density of  $150 \text{ mA cm}^{-2}$  and a temperature of  $410^\circ\text{C}$ . Figure 2b shows charge–discharge cycle testing. With a nominal cell voltage of 1.3 V over the duration of the test, which exceeded 100 cycles, the cell exhibited a coulombic efficiency of 92% and a round-trip energy efficiency of 71%. Moreover, this cell showed excellent rate capability, cycling at current densities as high as  $500 \text{ mA cm}^{-2}$  (Supplementary Fig. 1). Figure 3b,c shows

the underside of the negative electrode container. Plainly visible are droplets of metal identified by electron dispersive spectroscopy (EDS) to be Pb (Fig. 3d and Supplementary Fig. 2). This is clear

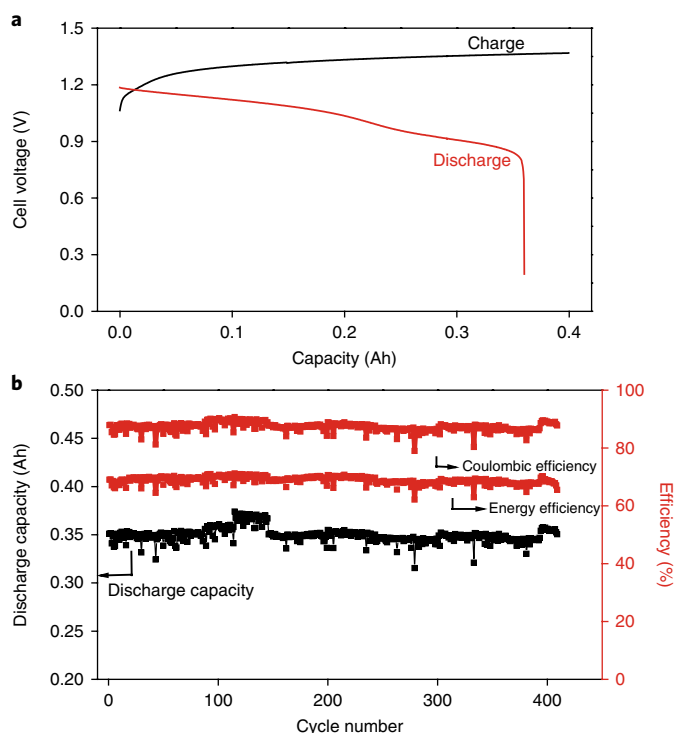


**Fig. 4 | Performance of a Mg–Pb||PbCl<sub>2</sub> cell.** **a**, Voltage–time traces, charge and discharge. **b**, Discharge capacity, energy efficiency and coulombic efficiency as a function of cycle number. Operating temperature,  $420^\circ\text{C}$ . Current density,  $100 \text{ mA cm}^{-2}$ .

evidence of the faradaic reaction that prevents irrecoverable loss of Pb into the negative electrode.

To quantify the effectiveness of the electronically conductive porous membrane, in a Li-Bi||PbCl<sub>2</sub> cell designed purposely to allow for easy detection of the presence of Pb in the negative electrode, the permeation rate of Pb<sup>2+</sup> was measured by direct-current plasma chemical analysis (Supplementary Fig. 3a). The nominal cell voltage was 1.1 V (Supplementary Fig. 3b), and the coulombic efficiency was measured to be 92.8%, similar to that of a cell fitted with a Li-Pb electrode. After different periods of continuous cycling, the concentration of Pb in Li-Bi was measured to determine the rate of Pb<sup>2+</sup> transport through the TiN faradaic membrane (Supplementary Table 1). If the loss of cell capacity were attributed solely to the permeation of Pb into the negative electrode, based on our measurements the corresponding capacity fade rate would be in the range of 0.00157% to 0.00192% per cycle, and the average capacity fade is 0.00172% per cycle (Fig. 3e). Of note is the observation that no Pb was found inside the TiN membrane in spite of the fact that its pore size is on the order of 10 to 20 μm (Supplementary Fig. 4), which is very large relative to the molecular scale. Clearly, steric hindrance is not the explanation for the exclusion of Pb. Instead, this is added proof that the TiN acts faradaically as an ion-selective membrane capable of blocking Pb<sup>2+</sup> while allowing transport of other ions (Li<sup>+</sup>, Cl<sup>-</sup>, K<sup>+</sup>). Put another way, electron transport through the matrix of TiN and charge transfer to Pb<sup>2+</sup> at the lower surface of the membrane are much faster than movement of Pb<sup>2+</sup> through the pores of TiN. The loss of capacity due to the blocking reaction is acceptably small as shown in Supplementary Fig. 5. If this battery were cycled daily, for example, to store solar energy harvested during the daytime for discharge during the night-time, 12 h rest time is representative. As loss of coulombic efficiency is directly linked to self-discharge, reducing the charging rate or increasing the charge capacity results in more severe self-discharge (Supplementary Tables 2 and 3). In fact, the blocking reaction can be shut off completely by slightly decreasing the operating temperature to freeze the electrolyte (Supplementary Fig. 6). In a demonstration of scalability, a membrane was fabricated of porous stainless steel and coated with TiN (Supplementary Figs. 7 and 8). This metal membrane was tested in a Li-Al||ZnCl<sub>2</sub> cell (Supplementary Fig. 9), which exhibited the same performance metrics as cells fitted with sintered TiN.

As proof of the applicability of the faradaically selective porous TiN membrane to a plurality of chemistries, we present test results of two other displacement batteries: Mg-Pb||PbCl<sub>2</sub> (Fig. 4) and Li-Al||ZnCl<sub>2</sub> (Supplementary Fig. 9), both configured identically to the Li-Pb||PbCl<sub>2</sub> cell described above. The Mg-Pb||PbCl<sub>2</sub> cell has a nominal cell voltage of 1.0 V and exhibits a coulombic efficiency of 90% and a round-trip energy efficiency of 70% over 400 cycles. Advantageously constructed of cheaper and environmentally friendlier metals, the Li-Al||ZnCl<sub>2</sub> cell has a nominal cell voltage of 1.3 V with a coulombic efficiency of 90% and a round-trip energy efficiency of 70%. After cycling, the TiN-coated porous stainless-steel membrane shows good chemical compatibility with molten salt and liquid metal in all instances (Supplementary Fig. 10).

## Conclusions

The use of a porous electronically conductive membrane, which achieves chemical selectivity by preferred faradaic reduction of vulnerable transition-metal ions rather than by regulated ion conduction, has been demonstrated successfully with a plurality of all-liquid displacement battery chemistries. It has not escaped our notice that the faradaically selective membrane reported here may have potential utility in other electrochemical devices (beyond energy storage) where delicate, ion-selective ceramic membranes are currently employed.

## Methods

**Preparation of the membrane.** A porous TiN membrane was prepared by sintering TiN powder mixed with 2 wt% MgO powder into a graphite crucible (OD: 2.54 cm, ID: 2.3 cm, height: 4.4 cm) with 16 holes (3-mm diameter) in the bottom. First, 5.8 g TiN powder (Alfa Aesar, 99.7%, < 10 μm) and 0.2 g MgO nanopowder (Inframat Advanced Materials) were mixed thoroughly by a pestle in an agate mortar for 30 min, and then the mixed powder was transferred into the perforated graphite crucible sitting on a flat stainless-steel plate to hold the powder in place. The powder mixture was then hand-pressed by a graphite rod to fill the graphite holes and confer some mechanical strength. In a second step, the assembly was transferred to a stainless-steel test vessel, and the test vessel was evacuated and purged with ultrapure Ar (99.999%) three times. Finally, the stainless-steel test vessel was blanketed with Ar and heated in a tube furnace to 1,100 °C at a ramping rate of 6 °C min<sup>-1</sup>. The temperature was maintained at 1,100 °C for 6 h. The specimen was then taken out of the furnace and cooled to room temperature.

A porous stainless-steel disc with a pore size of 20 μm (316 type, McMaster-Carr) was welded with a stainless-steel tube to make a crucible, and the TiN coating was applied by physical vapour deposition (Surface Solutions).

**Battery test.** A graphite crucible (OD: 3.8 cm, ID: 3.2 cm, depth: 4 cm) containing 7 g Pb (99.9%, Sigma Aldrich) was used as the positive electrode, and 15 g Pb contained in the TiN-fitted graphite crucible was employed as the negative electrode. A Pyrex glass or MgO ring (OD: 3.8 cm, ID: 2.6 cm, thickness: 0.5 cm) was positioned on top of the positive graphite crucible to support the negative graphite crucible and insulate the two electrodes from each other. The electrolytes were prepared with anhydrous lithium chloride (LiCl, 99.9%, ultradry, Alfa Aesar), sodium chloride (NaCl, 99.99%, ultradry, Alfa Aesar), potassium chloride (KCl, 99.95%, ultradry, Alfa Aesar) and magnesium chloride (MgCl<sub>2</sub>, 99.9%, ultradry, Alfa Aesar). The distance between the bottom of the TiN membrane and the inner bottom of the positive graphite crucible was 2 cm, and 35 g LiCl-KCl eutectic salt (Li/K = 0.592:0.408, atom ratio) was contained in the larger graphite crucible as electrolyte in between the electrodes. The cell was sealed in a test vessel filled with ultrapure Ar and heated by a tube furnace. The operating temperature of the cell was 410 °C measured by an ASTM type-K thermocouple. Galvanostatic charge/discharge testing was conducted with a battery test system (Arbin). A Mg-Pb||PbCl<sub>2</sub> cell had the same cell body, TiN membrane and positive electrode as the Li-Pb||PbCl<sub>2</sub> cell. The electrolyte composition was NaCl-KCl-MgCl<sub>2</sub> (Na/K/Mg = 0.271:0.221:0.508, molar ratio, eutectic temperature: 380 °C). A Li-Al||ZnCl<sub>2</sub> cell was assembled with a TiN-coated porous stainless-steel membrane as a separator (crucible diameter: 2.5 cm, pore size: 20 μm), LiCl-KCl molten-salt electrolyte, Al powder (particle size: 149 μm, 99%, Alfa Aesar) as the negative electrode, and Zn ingot (99.8%, Alfa Aesar) as the positive electrode. The cell was operated at 440 °C.

**Chemical analysis.** The permeation rate of Pb<sup>2+</sup> in the porous TiN membrane was measured in a Li-Bi||PbCl<sub>2</sub> cell. Except for the negative electrode, all cell components, such as cell body, TiN membrane and molten salt of the Li-Bi||PbCl<sub>2</sub> cell, were the same as that of the Li-Pb||PbCl<sub>2</sub> cell. The negative electrode of the Li-Bi||PbCl<sub>2</sub> cell, contained 20 g of Bi. The Pb concentrations of the Bi electrode after being cycled for 8, 23 and 41 days were measured by direct current plasma emission spectrometry by Luvac Laboratories.

**Materials characterization.** The microstructure of the sintered TiN membrane was characterized by a scanning electron microscope (SEM, JEOL 6610LV) fitted with an energy-dispersive spectrometer (EDS, IXRF systems, model 55i).

**Data availability.** The authors declare that the data supporting the findings of this study are available within the article and its Supplementary Information files.

Received: 20 July 2017; Accepted: 26 November 2017;  
Published online: 22 January 2018

## References

- Dunn, B., Kamath, H. & Tarascon, J.-M. Electrical energy storage for the grid: A battery of choices. *Science* **334**, 928–935 (2011).
- Soloveichik, G. L. Battery technologies for large-scale stationary energy storage. *Annu. Rev. Chem. Biomol. Eng.* **2**, 503–527 (2011).
- Yang, Z. G. et al. Electrochemical energy storage for green grid. *Chem. Rev.* **111**, 3577–3613 (2011).
- Barnhart, C. J. & Benson, S. M. On the importance of reducing the energetic and material demands of electrical energy storage. *Energy Environ. Sci.* **6**, 1083–1092 (2013).
- Kummer, J. T. & Weber, N. Battery having a molten alkali metal anode and a molten sulfur cathode. US patent 3,413,150 (1968).
- Coetzer, J. A. New high energy density battery system. *J. Power Sources* **12**, 377–380 (1986).
- Sudworth, J. L. The sodium/nickel chloride (ZEBRA) battery. *J. Power Sources* **100**, 149–163 (2001).

8. Lu, X. C., Xia, G. G., Lemmon, J. P. & Yang, Z. G. Advanced materials for sodium-beta alumina batteries: Status, challenges and perspectives. *J. Power Sources* **195**, 2431–2442 (2010).
9. Hueso, K. B., Armand, M. & Rojo, T. High temperature sodium batteries: status, challenges and future trends. *Energy Environ. Sci.* **6**, 734–749 (2013).
10. Benato, R. et al. Sodium nickel chloride battery technology for large-scale stationary storage in the high voltage network. *J. Power Sources* **293**, 127–136 (2015).
11. Kim, J., Jo, S. H., Bhavaraju, S., Eccleston, A. & Kang, S. O. Low temperature performance of sodium-nickel chloride batteries with NaSICON solid electrolyte. *J. Electroanal. Chem.* **759**, 201–206 (2015).
12. Lu, X. et al. High power planar sodium-nickel chloride battery. *ECS Trans.* **28**, 7–13 (2010).
13. Lu, X. C. et al. Advanced intermediate-temperature Na–S battery. *Energy Environ. Sci.* **6**, 299–306 (2013).
14. Lu, X. C. et al. Liquid-metal electrode to enable ultra-low temperature sodium-beta alumina batteries for renewable energy storage. *Nat. Commun.* **5**, 4578 (2014).
15. Gasior, W. & Moser, Z. Thermodynamic study of liquid lithium-lead alloys using the EMF method. *J. Nucl. Mater.* **294**, 77–83 (2001).
16. Wang, K. et al. Lithium-antimony-lead liquid metal battery for grid-level storage. *Nature* **514**, 348–350 (2014).

## Acknowledgements

We acknowledge financial support from Total, S.A.

## Author contributions

H.Y., B.C., F.C. and T.O. contributed equally to this work. D.R.S., B.C., H.Y. and T.O. conceived of the idea for the project. H.Y., B.C., F.C., T.O., J.Z. and N.T. constructed the battery and conducted the tests. F.C., J.Z., N.T. and H.Y. prepared the TiN membrane. T.O. verified the stability of TiN in this cell. H.Y., B.C., T.O. and D.R.S. prepared the manuscript.

## Competing interests

The authors declare no competing financial interests.

## Additional information

**Supplementary information** is available for this paper at <https://doi.org/10.1038/s41560-017-0072-1>.

**Reprints and permissions information** is available at [www.nature.com/reprints](http://www.nature.com/reprints).

**Correspondence and requests for materials** should be addressed to D.R.S.

**Publisher's note:** Springer Nature remains neutral with regard to jurisdictional claims in published maps and institutional affiliations.